EXPERIMENTAL RESONANCE STUDIES AT THE ESR

A. Sherjan*[1,2], G. Franchetti[1,2,3], J. Rausch[2]
[1]GSI Helmholtz Centre for Heavy Ion Research, Darmstadt, Germany
[2]Goethe University Frankfurt, Frankfurt am Main, Germany
[3]Helmholtz Research Academy Hesse for FAIR, Frankfurt am Main, Germany

Abstract

The storage ring ESR at GSI unlocks the possibility for various atomic physics experiments with exotic beams. Therefore the operation of the ESR requires a wild change of parameters and cycles. This may inadvertently push the machine tunes to cross a nonlinear resonance. This is particularly important in the process of deceleration, where the machine tune is moving quite notably along the cycle as measurements have shown, which could be one of the causes of significant beam loss. Consequently, it is relevant to retrieve the actual resonance chart for the ESR. In this proceeding we discuss the adopted procedure, in the light of the ESR complexity and the limited coverage in the tune diagram for the implemented inverse tune response matrix in the machine settings, providing a first correction method.

MOTIVATION

The ESR as a storage ring offers a variety of highly charged heavy ion beams at different energies, for which in many cases the beam needs to be decelerated [1]. In the process of deceleration a considerable amount of the beam is lost, while at the same time the machine performs significant tune and closed orbit swings [2]. Both could be measured during the Machine Development (MD) 2024 as a first characterization of the beam loss during the deceleration. As a follow-up in the MD 2025, efforts were made to acquire experimentally more information about the present state of the machine in order to improve the existing model of the ESR [2–4]. During the same measurement campaign a first attempt to measure the ESR resonance chart at injection energy has been carried out. This chart is a useful tool to reveal possible sources of beam loss during deceleration [5].

MEASUREMENT

To ensure that the measurements cover effectively a wide range in the tune diagram, the beam needs to be injected at different working points (WPs) of the machine, which are ideally distributed in a rectangular grid. Then the tune is moved along the grid lines, while the beam intensity is simultaneously stored. Step-like changes in the recorded beam intensity mark the positions in the tune diagram where resonance lines were crossed, see Fig. 1. A preliminary test on possible injection WPs have shown that only two WP could be found to perform the measurements, see Fig. 2 (left). Attempts to inject in all other WPs led to immediate full beam loss. Therefore the tune scan could not be carried out in a grid-like pattern, but instead starting only from these two WPs, with the results shown in Fig. 2. This limitation affects the region that we can explore in the tune diagram. The measured points of crossing resonances are depicted in red in Fig. 2. These points are seemingly located on distinct lines, but if compared with the theoretical resonance chart, they cannot be clearly mapped to any resonance line, see Fig. 2 (right).

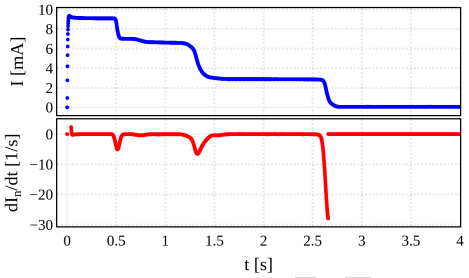

Figure 1: Above: Beam intensity is measured simultaneously, while the LSA tunes (Q_x^L, Q_y^L) are changed from $(2.45, 2.35)$ to $(2.4, 2.25)$. Below: The peaks in the normalized change of the beam intensity localize the positions of resonance crossing in the tune diagram.

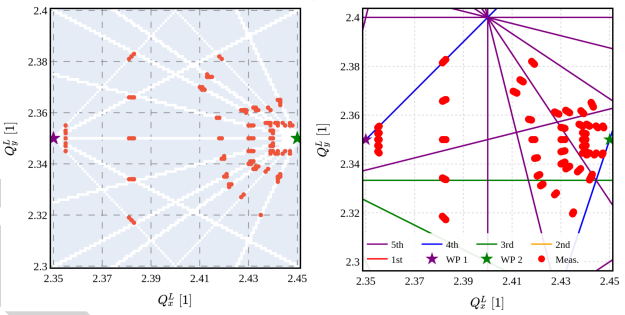

Figure 2: Left: Tune scan paths in the tune diagram, starting from the only two injectable WPs marked with stars. Red points depict positions of measured resonance crossings. Right: Same results plot into the web of theoretically possible resonance lines.

FORWARD MAP

To retrieve the experimental resonance chart, the tune values (Q_x^L, Q_y^L) were not measured, but taken from the LSA (LHC Software Architecture) settings [6]. Hence, the next step is to check, if the discrepancies between measured and theoretically possible resonance lines, are related to the inverse tune response matrix, R^{-1}, implemented in the settings of the control system [7]. This matrix maps the intended change of the LSA tunes $\Delta Q^L = (\Delta Q_x^L, \Delta Q_y^L)$, to the re-

* a.sherjan@gsi.de

quired change of the focusing strengths of the quadrupole families Δk, namely $\Delta k = R^{-1} \cdot \Delta Q^L$. In the ESR the change of tune acts on the strength of all the quadrupoles, which are grouped in 5 families. Figure 3 shows the relation between the LSA tunes, (Q_x^L, Q_y^L), which are changed by choice along a well defined grid and the corresponding simulated ESR tunes,(Q_x, Q_y), after the strength of the quadrupole families were set according to the matrix R^{-1}. Note, that the coloring

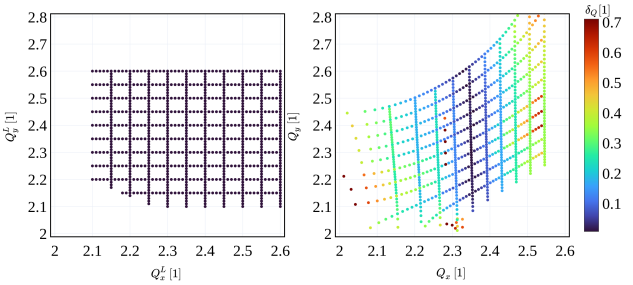

Figure 3: Left: Regular grid in the (Q_x^L, Q_y^L) tune diagram chosen as the input of the forward map f. Right: Output grid of corresponding machine tunes (Q_x, Q_y) is distorted after applying f.

of Fig. 3 is chosen to be an average of the relative deviation between the LSA tune and the machine tune in both planes as follows

$$\delta_Q = \frac{1}{2}\left(\left| \frac{Q_x^L - Q_x}{Q_x} \right| + \left| \frac{Q_y^L - Q_y}{Q_y} \right| \right) . \qquad (1)$$

With this color representation, the level of agreement between LSA- and machine tune can be highlighted, from dark color for full agreement to lighter color for less agreement (see the right plot of Fig. 3). Figure 3 is the graphical representation of the function f describing the forward map which relates to each pair of LSA tune values (Q_x^L, Q_y^L) the corresponding simulated ESR values (Q_x, Q_y), namely $f : (Q_x^L, Q_y^L) \mapsto (Q_x, Q_y)$. As can be seen, the implemented matrix R^{-1} is accurate in a small region around the WP of the machine, here at $(Q_x, Q_y) \approx (2.351, 2.307)$, and differs more the further away from it, especially in the direction of Q_x. This limits the applicability of the matrix R^{-1} to only a small area around the initial WP. This has also implications on the position of resonance lines, where their location would be expected with respect to where they actually are in the resonance chart due to the distortion of the tune diagram created by the settings of R^{-1}.

INVERSE MAP

In order to obtain how the theoretical web of resonance lines in the (Q_x, Q_y) tune diagram appear in the LSA set tunes (Q_x^L, Q_y^L), the forward map f needs to be applied on a very well resolved grid in (Q_x^L, Q_y^L). Then the inverse map, f^{-1}, can be obtained using backwards the same data base, hence numerically we find $f^{-1} : (Q_x, Q_y) \mapsto (Q_x^L, Q_y^L)$, which is shown in Fig. 4 for the mapping of theoretical resonance lines on LSA-tunes. Note that f maps a regular grid on a new one which is irregular, see Fig. 3. Therefore each pair (Q_x, Q_y) on the theoretical resonance lines is approximated by the closest grid point of the irregular to find the inverted map, and clearly this compromises the resolution of f^{-1} and affects the line width of the inverted resonance lines in Fig. 4. Figure 4 shows enormous deviations between the

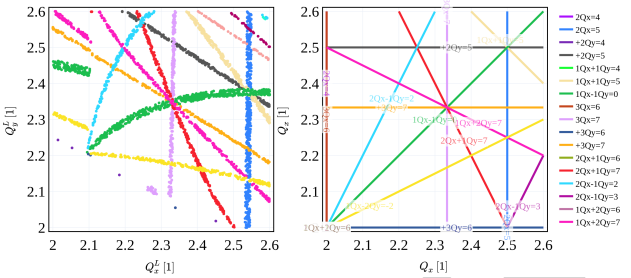

Figure 4: Left: The web of theoretical resonance lines is used for the inverse map f^{-1} and shows strong deformations to the right picture resonance chart. Right: Theoretical resonance chart for comparison.

expected resonance lines without distortion (right) and the LSA-retrieved resonance lines based on the implemented matrix R^{-1} (left) regarding the position, shape and orientation of each resonance line. For example, the horizontal lines in the theoretical resonance chart become diagonal in the (Q_x^L, Q_y^L) diagram and vice versa. We observe that the function f, retains the property that each line intersection consists of the same lines in comparison with the theoretical model. Lastly we plot in Fig. 5 the LSA-retrieved experimental resonance points on this distorted resonance chart, to see if the ESR resonance lines can be identified. The plot shows that there is still a discrepancy between measurements and theoretical lines.

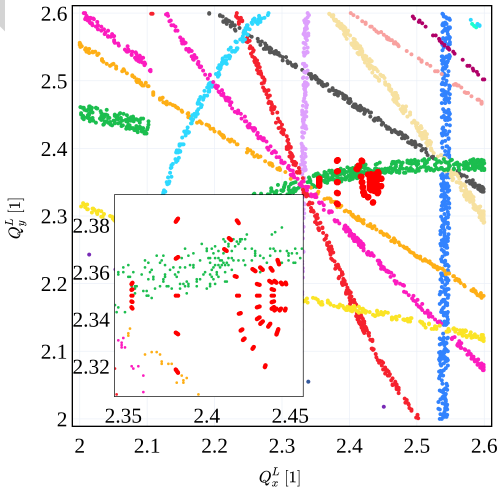

Figure 5: The LSA-retrieved location of measured beam loss plotted in the inverted theoretical resonance chart appears to have no overlap with any low order resonance line.

CORRECTION METHOD

In the following, a simple first order correction of the matrix R^{-1} will be discussed. As Fig. 3 suggests, the forward

map f leads approximately to a linear tilt of all horizontal lines. Therefore the approach is to determine the average slope of these lines, see Fig. 6 left and apply: first the inverted slope on the LSA tunes and second the function f, so that both operations compensate each other in linear approximation. In a few iterations of calculating the average inverse slope and correcting the LSA tunes accordingly, this method can be optimized to yield an improvement in the Q_y direction, which is presented in Fig. 6 right. Clearly, an additional correction along the Q_x would be needed to improve also the other direction, as still the tune grid is stretched towards the integer tune and compressed towards the half integer tune. However, considering the simplicity of this approach the correction is efficient enough for the moment to check in the following the impact of a correction of this order. Therefore, according to the discussed procedure, the

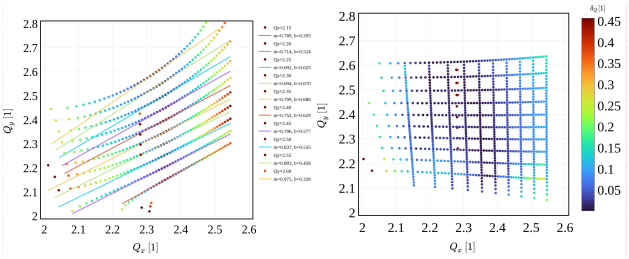

Figure 6: Left: Determining the slope of each tilted horizontal line. Right: Tune grid after the correction is more regular and in stronger agreement to the LSA set tunes.

inverted theoretical resonance chart, is mapped again, now including the R^{-1} correction, which results in a better agreement between both tune representations, see Fig. 7. After the R^{-1} correction, the horizontal and diagonal resonance lines for example keep their orientation. Note, that also the width of the lines has become sharper given the same resolution size of the input grid. As mentioned before, the limits of this correction are also visible in the remaining deviation of the resonance lines along Q_x^L due to the missing correction in the other plane.

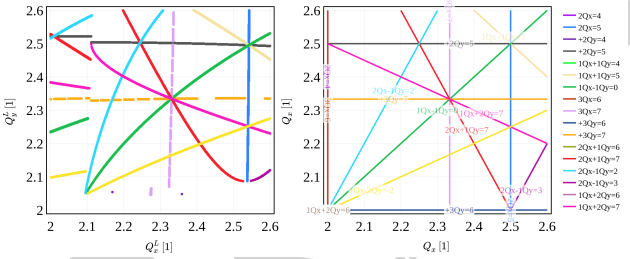

Figure 7: Left: Inverted theoretical resonance chart with R^{-1} correction is now in better alignment with the original resonance chart (right picture). Right: Theoretical resonance chart for comparison.

DYNAMIC APERTURE

Lastly, we compute the dynamic aperture (DA) on the example of the ESR bare lattice, including the sextupole magnets, but neglecting further high order perturbation in the magnetic field of each component. Figure 8 shows, as expected, that also the calculations on the DA greatly benefit by the R^{-1} correction as they are in better alignment, especially along Q_y. This picture also reveals a strong reduction of the DA for WPs close to the horizontal integer.

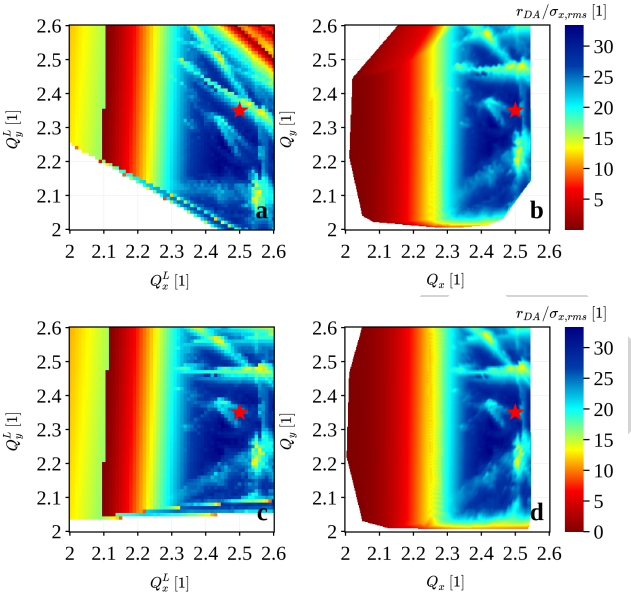

Figure 8: a) DA vs (Q_x^L, Q_y^L) without R^{-1} correction; b) DA vs (Q_x, Q_y) as in the machine. c) DA vs (Q_x^L, Q_y^L) but now with implemented the R^{-1} correction. d) DA vs (Q_x, Q_y) with same R^{-1} correction. The simulations are done for a reference beam with rms emittance of $\epsilon_{\text{x,rms}} = 5$ mm-mrad.

CONCLUSION

The way the inverse tune response matrix R^{-1} is chosen to set the strength of the quadrupole families in the machine for a required change of the LSA tunes, can enhance or reduce the discrepancy between the set and the targeted tune. This effect is large when setting for larger tune differences around the reference WP. The discrepancy between the LSA tune and the machine tune cannot be neglected when the machine tune is subject to change during operation (to avoid resonance crossing). Hence, further improvement with the presented first order correction for the matrix R^{-1} can be achieved and needs to be developed with a more accurate nonlinear fit of the inverse map. This improvement will allow to retrieve a more reliable experimental resonance chart, which can be compared with the prediction of an ESR model of the nonlinear lattice. This validation is essential for modeling machine performance during deceleration.

ACKNOWLEDGMENTS

The authors would like to thank David Ondreka, Holger Liebermann, Carsten Mühle and Oleksandr Chorniy for the exchange and support and to thank the ESR operation team for the preparation of the machine for the experiments.

REFERENCES

[1] B. Franzke, "The heavy ion storage and cooler ring project ESR at GSI," *Nucl. Instrum. Methods Phys. Res. B*, vol. 24–25, pp. 18–25, 1987. doi:10.1016/0168-583X(87)90583-0

[2] A. Sherjan, G. Franchetti, J. Rausch, and B. Lorentz, "Measurements and studies on the nonlinear Dispersion in the ESR", presented at IPAC'26, Deauville, France, May 2026, paper THP4076, this conference.

[3] A. Heinz, G. Franchetti, A. Sherjan, J. Rausch, and B. Lorentz, "Beam based optimization of the ESR linear optics model", presented at IPAC'26, Deauville, France, May 2026, paper WEP5015, this conference.

[4] J. Rausch, A. Sherjan, G. Franchetti, and B. Lorentz, "Retrieving the longitudinal nonlinear tunes from FCT measurements", presented at IPAC'26, Deauville, France, May 2026, paper THP4076, this conference.

[5] G. Franchetti *et al.*, "Experiment on space charge driven nonlinear resonance crossing in an ion synchrotron", *Phys. Rev. ST Accel. Beams*, vol. 13, no. 11, p. 114203, Nov. 2010. doi:10.1103/PhysRevSTAB.13.114203

[6] C. Roderick and R. Billen, "The LSA database to drive the accelerator settings", CERN, Geneva, Switzerland, Rep. CERN-ATS-2009-100, Nov. 2009. https://cds.cern.ch/record/1215575

[7] D. Ondreka, "LSA optics – version 0.2", GSI Helmholtzzentrum für Schwerionenforschung. https://web-docs.gsi.de/~weick/frs/SYS_Ondreka_LSA_Optics_v0.2.pdf